Anion Effects on the Kinetics of Mercury Underpotential Deposition on Au(111) Electrodes

E. Herrero and H. D. Abruña*

Department of Chemistry, Baker Laboratory, Cornell University, Ithaca, New York 14853-1301

Received: September 4, 1997; In Final Form: October 25, 1997[⊗]

The kinetics and mechanism of mercury underpotential deposition (UPD) on Au(111) electrodes have been investigated in the presence and absence of strongly interacting anions including bi-sulfate, chloride, and acetate. In the absence of strongly interacting anions, i.e. in perchloric acid, the mercury UPD process is largely controlled by mercury−gold surface interactions. The presence of sulfuric acid in the supporting electrolyte alters the kinetics of the initial and final stages of mercury deposition/dissolution. The presence of two well-ordered structures at potentials below (a mercurous sulfate $\sqrt{3}\times\sqrt{19}$ structure) and above (a $\sqrt{3}\times\sqrt{7}$ bi-sulfate structure) mercury deposition leads to the appearance of two pairs of sharp spikes in the cyclic voltammogram. Analysis of the current transients obtained for deposition and dissolution processes reveals that three different processes are taking place during the adsorption/desorption of the mercury bi-sulfate layer: adsorption/desorption processes governed by Langmuir kinetics, a nucleation and growth process linked to an order/disorder transition to form the mercury bi-sulfate adlayer, and an order/disorder transition related to the formation/disruption of the $\sqrt{3}\times\sqrt{7}$ bi-sulfate layer. In chloride medium, the voltammetric profile is very similar to that obtained in sulfuric acid solution, with the presence of two sharp spikes. However, no nucleation and growth kinetics mechanism was found linked to the process of formation/disruption of the mercury chloride adlayer. The transients show a clear deviation from the ideal Langmuir behavior, probably associated with the presence of attractive interactions in the mercury chloride adlayer. The kinetics of mercury UPD in acetate media are significantly slower than in the previous media, as revealed by voltammetric and chronoamperometric measurements. The slow kinetics appear to be related to the formation of Hg^{2+}−acetic acid complexes in solution. Although ordered structures are formed at potentials below the main UPD peak, no nucleation and growth mechanism was observed.

1. Introduction

The underpotential deposition (UPD) of metals onto foreign metal substrates offers the opportunity for studying the early stages of metal deposition.[1,2] In recent years, the use of single-crystal electrodes in conjunction with in situ surface techniques, including scanning tunneling microscopy (STM),[3−6] atomic force microscopy (AFM),[7,8] and surface X-ray-based techniques,[8−13] has allowed a detailed investigation of UPD processes. Of particular importance in this regard has been the ability to characterize the different surface structures formed at different potentials and to correlate them with their voltammetric behavior. However, kinetic studies of UPD processes have received considerably less attention.[14−21] Such studies are especially revealing and valuable when detailed potential-dependent structural information is available, since it allows for a direct correlation of the different surface structures with the kinetics of the processes involved. However, the number of studies where kinetic and structural information is available is quite limited. In one such example, Kolb and co-workers[20,21] have investigated the kinetics of copper UPD on Au(111) electrodes and have made correlations with structural information. They found that the process followed an instantaneous nucleation mechanism, likely controlled by the density of defect sites on the surface.

In this paper we present a study of the kinetics of mercury UPD on Au(111) electrodes and employ previous structural studies to arrive at a more detailed description of the electrodeposition process. Several structural studies of mercury UPD on Au(111) electrodes have been carried out, using AFM,[22] STM,[23] and X-ray based techniques.[24−26] This system exhibits a marked anion dependence of the surface structures.[22,26] In sulfuric acid, several well-ordered structures have been found, including a ($\sqrt{3}\times\sqrt{19}$) mercurous sulfate bilayer at potentials between +0.80 and +0.88 V[23,24] and, additionally, two different incommensurate and commensurate hexagonal structures at potentials between +0.68 and +0.63 V and below +0.63 V, respectively.[25] At potentials above the main UPD peaks, Itaya and co-workers determined that the adsorbed bi-sulfate presents an ordered ($\sqrt{3}\times\sqrt{7}$) structure.[23] In chloride media, no ordered surface structure has been found after the mercury UPD peaks.[26] However, crystal truncation rod (CTR) measurements indicate that the adlayer is composed by mercury species and chloride anions, forming a bilayer likely in the form of Hg_2Cl_2.[26] At potentials positive to the main UPD peaks (and in the absence of Hg ions in solution) an ordered hexagonal chloride structure was found by Ocko and co-workers using surface X-ray scattering techniques.[27] Ordered mercury structures have also been found in acetate buffer after the main UPD peak.[26] The deposited mercury acetate species forms an incommensurate hexagonal structure that compresses irreversibly as the potential is made progressively more negative. In some cases, the formation of such ordered phases is reflected on the cyclic voltammetric profile.[28]

As mentioned above, in this work we examine the kinetics of the deposition/dissolution of the different mercury adlayers formed on Au(111) electrodes in sulfuric acid, chloride, and

[⊗] Abstract published in *Advance ACS Abstracts,* December 15, 1997.

S1089-5647(97)02891-5 CCC: $15.00
Published on Web 01/08/1998

acetate buffer containing electrolytes. The behavior in the presence of these anions is compared and contrasted with that obtained in perchloric acid, where virtually no influence of the anions is expected in the UPD process.

2. Experimental Section

Two different sized Au(111) electrodes were employed in these studies. The larger one (of ca. 0.9 cm diameter) was grown from the melt at the Materials Science Center at Cornell University and was cut and polished with a miscut of less than 0.3°. The smaller crystal (of ca. 2 mm diameter with an area approximately 25 times smaller than the previous electrode) was prepared according to Claviler's technique with a miscut of less than 0.1°. Prior to any measurement, the electrodes were flame annealed, quenched with ultrapure water,[29] and transferred to the cell for electrochemical measurements.

Cyclic voltammetric and potential step chronoamperometric measurements were carried out in a U-shaped two-compartment electrochemical cell in the hanging meniscus configuration. Particular care was taken to minimize iR drops so that the current transients would not be affected. The transients obtained with both electrodes were the same, in both current density and shape, a clear indication that iR drops are not affecting the measurements. Electrochemical experiments were carried out with a PAR 283 potentiostat interfaced with Corrware software.

For the desorption (adsorption) chronoamperometric current transients, the potential was stepped from an initial potential where the mercury adlayer was completely formed (desorbed) to a final potential were partial or total desorption (partial or complete adsorption) took place. In a series of experiments, the final potential is increased (decreased) in 2 mV steps from a potential corresponding to the initial stages of the desorption (adsorption) to the complete desorption (adsorption).

All potentials were measured versus a Ag/AgCl electrode in 3 M NaCl. A large area coiled gold wire was used as a counter electrode. All experiments were carried out at room temperature. Solutions were prepared using ultrapure water (18 MΩ Millipore Milli-Q water), $HClO_4$ (doubly distilled, 70%, GFS Chemicals), H_2SO_4 (Ultrex J. T. Baker), NaCl (99.999%, Aldrich), CH_3COOH (99.9985%, Alfa), CH_3COONa (99.999%, Alfa), and HgO (99.998%, Alfa).

3. Results and Discussion

3.1. Cyclic Voltammetry. Cyclic voltammograms of mercury UPD on Au(111) electrodes in four different supporting electrolytes and at a solution mercury concentration of 1.0 mM are shown in Figure 1, together with the stability ranges of the different structures found in these media. In these four different electrolytes, the effect of the anion on the UPD process is clearly evident. In the absence of strong adsorbing anions (i.e., in 0.1 M $HClO_4$), only one pair of peaks with a Gaussian-like shape appears in the voltammetric profile (Figure 1A). The peak shape suggests that in this medium the mercury adsorption−desorption processes are governed by a Langmuir isotherm in which the interactions between the surface gold atoms and the mercury adatoms play the dominant role. In the presence of strongly adsorbing anions (Figure 1B−D), there are changes in the peak shape and position which, in turn, reflect changes affecting the kinetics and the interactions between the species involved in the UPD process.

The cyclic voltammetric response in sulfate and chloride media are quite similar (Figure 1B,C), particularly over the potential range comprising the main UPD peaks. When compared to the profile in perchloric acid, the peak positions

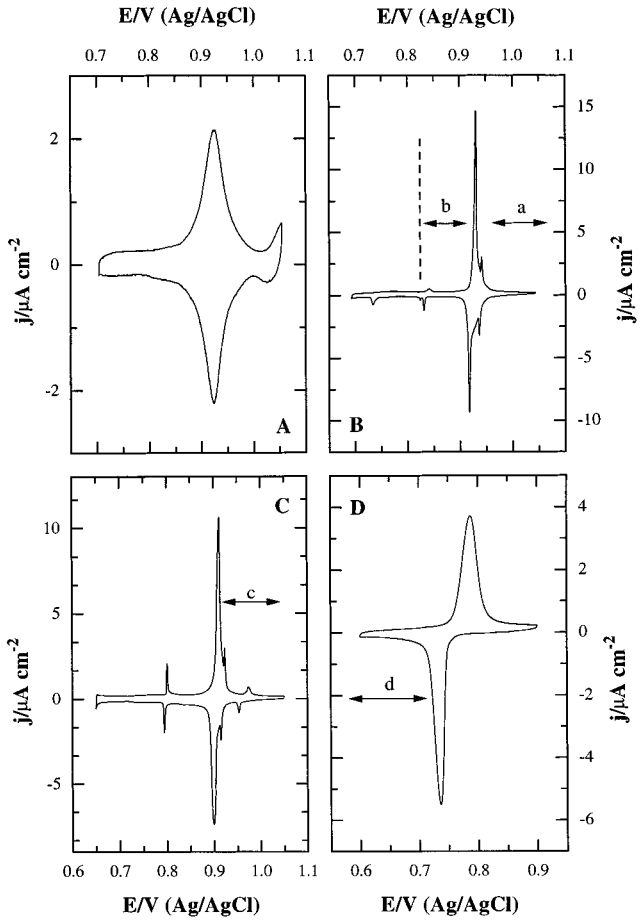

Figure 1. Voltammetric profile for a Au(111) electrode in (A) 0.10 M $HClO_4$ +1.0 mM Hg^{2+}, (B) 0.10 M H_2SO_4 + 1.0 mM Hg^{2+}, (C) 0.10 M $HClO_4$ + 1.0 mM NaCl + 1.0 mM Hg^{2+}, and (D) 0.10 M CH_3COOH + 0.10 M CH_3COONa + 1.0 mM Hg^{2+}. Scan rate: 1 mV s^{-1}. The arrows indicate the stability region for the different ordered structures. See text for notation.

do not change significantly, indicating that the main interaction is still mercury−gold. However, instead of the broad voltammetric peak present in perchloric acid medium, there are two new well-defined and sharp pairs of peaks. The very sharp peaks that appear at the onset of mercury deposition can be ascribed to an order-to-disorder transition in the anion adlayer. At potentials positive of the mercury UPD deposition, sulfate and chloride are adsorbed on the electrode surface forming ordered adlayers: $\sqrt{3}\times\sqrt{7}$[23] (region a in Figure 1B) and hexagonal[27] (region c in Figure 1C), respectively. The initial stages of mercury deposition trigger an order-to-disorder transition that gives rise to the sharp spikes.[28]

The main difference between sulfate and chloride media is found at potentials negative of the main UPD peaks. Whereas in situ X-ray[24] and STM[23] studies have found ordered adlayers immediately after the main UPD peaks in sulfuric acid, X-ray measurements have failed to identify any ordered structure in chloride media.[26] In sulfuric acid, a ($\sqrt{3}\times\sqrt{19}$) mercurous sulfate structure has been reported between +0.80 and +0.88 V (region b in Figure 1B). In spite of that, the shape of the voltammetric peak is quite similar in both media, with sharp peaks at very similar potentials at the final stages of the UPD process. The full width at half-maximum (ΔE_{fwhm}) of the voltammetric peaks in both sulfate and chloride media is significantly smaller than the value obtained in perchloric acid (ca. 45 mV), suggesting the presence of significant attractive lateral interactions in the presence of sulfate and chloride relative

to perchlorate. The formation of a mercury−anion bilayer (with mercury likely present as mercurous dimers) observed with CTR measurements is also consistent with these assertions.[24,26]

In acetate buffer, mercury UPD on Au(111) electrodes exhibits behavior that is completely different from that found in the other supporting electrolytes. The first significant difference is a change in the potential for mercury UPD. The main deposition peaks in this medium are shifted by over 100 mV, toward negative potentials, relative to all the other supporting electrolytes studied. This change reflects a significant modification in the interactions governing the UPD process that results in a hindering of the mercury UPD process. This could arise as a result of either strong anion (acetate) adsorption on the gold electrode surface prior to the UPD process or the formation of mercuric complexes. A displacement of more than 100 mV in the deposition peak would suggest that acetate is more strongly adsorbed on gold surfaces than chloride anions, which we do not believe is a likely situation. On the other hand, Hg^{2+} and acetic acid form stable complexes in aqueous solutions (up to a 1:4 stoichiometry).[30] The formation of such complexes would stabilize the Hg^{2+} species in solution, giving rise to a negative displacement in the deposition potential. At potentials negative of the main deposition peak, an ordered incommensurate hexagonal adlayer composed of mercury species and acetate anions has been observed by X-ray measurements[26] (region d in Figure 1D). This adlayer exhibits an irreversible compression as the potential is made progressively more negative.

Another important characteristic of the cyclic voltammogram in acetate buffer is the peak separation for the deposition and stripping processes. Even at scan rates as low as 1 mV s^{-1} the peak separation is about 50 mV, a clear indication of very slow adsorption/desorption kinetics. The dissociation of Hg^{2+}−acetic acid complexes is likely responsible for the slow kinetics.

3.2. Current Transient Measurements. It is evident that anions significantly affect the kinetics of the adsorption/desorption processes of mercury UPD on Au(111) electrodes. In sulfate, chloride, and acetate media, CTR measurements suggest that a bilayer is formed on the electrode surface following mercury deposition.[24,26] This bilayer is composed of mercurous dimers bonded directly to the electrode surface with anions adsorbed on top of the mercury adlayer. In sulfate and acetate media, this type of arrangement leads to the formation of ordered structures on the electrode surface. However, in the presence of chloride, no ordered structure could be found by grazing incident X-ray diffraction.[26] We now embark on a discussion of the kinetics of the formation/dissolution of these bilayer structures formed on Au(111) electrodes in the course of mercury UPD processes.

The formation and dissolution of ordered adlayers often leads to order/disorder transitions, which generally occur through a nucleation and growth mechanism. In order to investigate such a possibility, current transients for the adsorption and desorption processes were recorded. The transients in the presence of sulfate, chloride, and acetate are compared to those obtained in 0.1 M $HClO_4$. From the voltammetric behavior, we know that the UPD process in this last medium is governed by Langmuir-type kinetics, and as anticipated, all the current transients obtained in this medium exhibited an exponential decay of the current after the potential step.

Current Transients in 0.1 M H_2SO_4. Figure 2 shows four different desorption transients (out of 26 taken) for the mercury UPD process recorded in 0.1 M H_2SO_4 + 1.0 mM Hg^{2+}. In these transients, the electrode was stepped from +0.898 to +0.928 (A), +0.938 (B), +0.942 (C) and +0.946 V (D). As can be seen, only the transient in Figure 2A has an exponential-type decay that can be associated to a process that follows Langmuir desorption kinetics. All the other transients exhibit one (Figure 2B,C) or two (Figure 2D) shoulders superimposed on the exponential decay. This behavior contrasts that obtained in perchloric acid where an exponential decay, similar to that shown in Figure 2A, was obtained over the entire range of potentials examined.

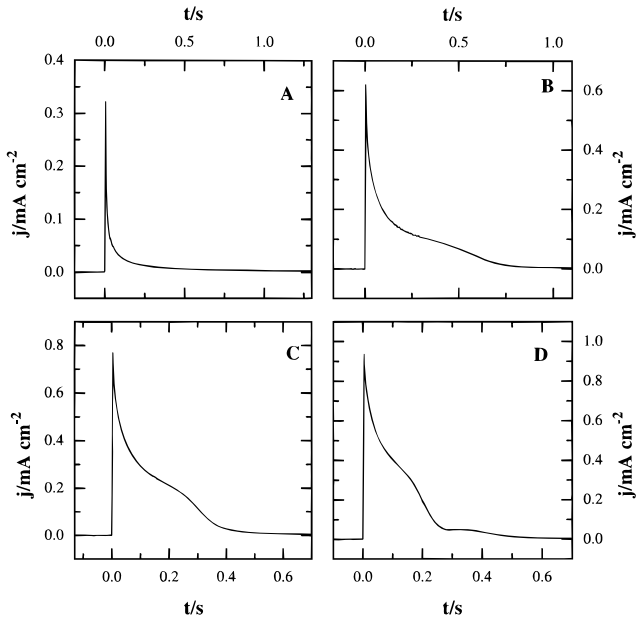

Figure 2. Current transients for mercury desorption processes on a Au(111) electrode for potential steps from +0.898 V to (A) +0.928, (B) +0.938, (C) +0.942, and (D) +0.946 V in 0.10 M H_2SO_4 + 1.0 mM Hg^{2+}.

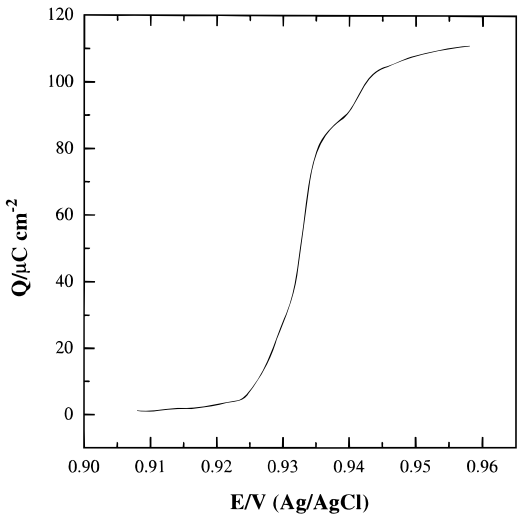

Figure 3. Charge isotherm obtained from the desorption current transients in 0.10 M H_2SO_4 + 1.0 mM Hg^{2+}.

The charge underneath the desorption transients was measured in order to obtain the charge isotherm for the desorption process (Figure 3). This charge isotherm could have also been obtained from the voltammetric profile through integration. Aside from the small differences between the deposition and dissolution processes exhibited in the cyclic voltammogram at 1 mV s^{-1}, the charge isotherm obtained from it should have the same characteristics. However, since the voltammetric profile has more distinctive features than the charge isotherm, a better comparison between both techniques is achieved when the

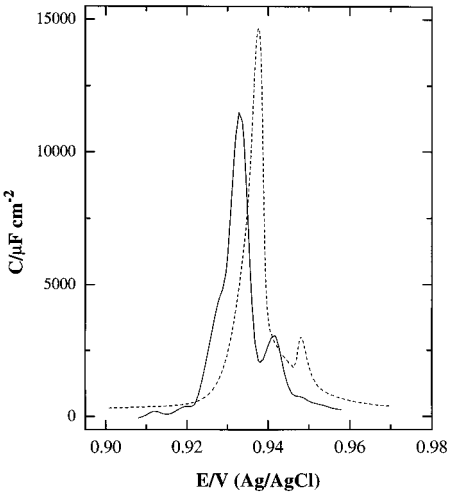

Figure 4. Capacitance profile form the charge isotherm (full line) and the voltammetric profile (dashed line) for mercury desorption in 0.10 M H_2SO_4 + 1.0 mM Hg^{2+}.

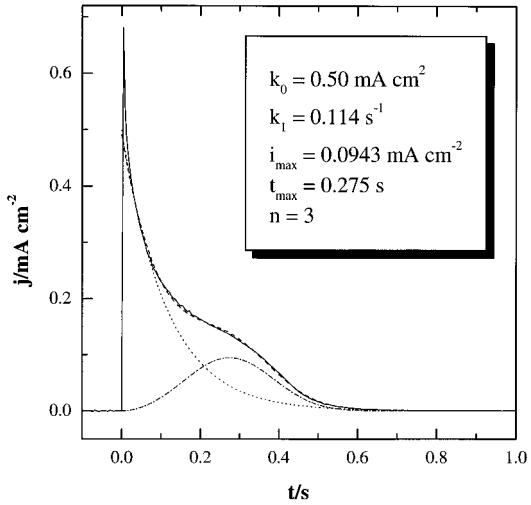

Figure 5. Current transient for mercury desorption processes on a Au(111) electrode for a potential step from +0.898 to +0.938 V (full line) and fitted curve with a progressive nucleation model (dashed line) in 0.10 M H_2SO_4 + 1.0 mM Hg^{2+}. The dotted and dash-dotted lines represent the Langmuir and nucleation and growth terms, respectively. Values of the parameters obtained from the fitting are given in the inset.

charge isotherm is differentiated to give the capacitance curve. The capacitance curve is easily obtained from the voltammetric profile by dividing the current density by the scan rate. Figure 4 presents the capacitance curve obtained from the charge isotherm (full line) and that obtained from the cyclic voltammogram (dashed line). As can be seen, all the voltammetric features are present in the capacitance curve obtained from the charge isotherm. There are only two small differences to note. First, the peaks in the capacitance curve obtained from the charge isotherm are shifted negatively by about 4−8 mV relative to those in the cyclic voltammetry. As mentioned above, the cyclic voltammetric profile exhibits some irreversibility that results in the shifting of the desorption peaks toward positive values relative to the equilibrium potential. Since the charge from the transients reflects a quasi-equilibrium state, the differences in peak positions are the result of the irreversibility in the cyclic voltammetric profile. Second, the lower resolution of the charge isotherm (2 mV) relative to the voltammetric profile (0.1 mV) gives rise to a main peak with lower amplitude.

An analysis of the current transients can provide information on the kinetics of the processes involved. Previous voltammetric[28] and X-ray measurements[24,26] have revealed the existence of three different processes consisting of two order/disorder transitions (at the onset and at the end of the desorption processes, respectively) and the desorption process that follows a Langmuir-type isotherm. The presence of a nucleation and growth mechanism is suggested by the shoulders present in the transients. In fact, the potential at which these shoulders appear in the transients matches precisely the peak positions in the capacitance curve. However, since the order/disorder transitions occur concurrently with a Langmuir-type desorption process, the shape of the current transients will not necessarily be that expected for a nucleation and growth process alone.

Transients with only one shoulder should be described by an expression containing a Langmuir kinetics term plus a nucleation and growth kinetics term. For the nucleation and growth process the Bewick-Fleischmann-Thirsk (BFT) model will be used in the present case.[31,32] In this approach the equation for the transient is given by

$$j = k_0 \exp(-k_1 t) + j_{\max}\left(\frac{t}{t_{\max}}\right)^{n-1} \exp\left[\left(\frac{1-n}{n}\right)\left(\frac{t}{t_{\max}}\right)^{n} - 1\right] \quad (1)$$

where the fist term corresponds to the Langmuir kinetics and the second to nucleation and growth. k_0 and k_1 are the parameters for the Langmuir process, j_{max} is the maximum current density for the nucleation and growth process, t_{max} is the time at j_{max} and n is a parameter related to the nucleation mechanism. Generally an n value of 2 indicates an instantaneous nucleation process whereas an n value of 3 would be indicative of a progressive nucleation process. This equation was used to fit all the experimental results in order to obtain the kinetic parameters.

In this model, the processes giving rise to the Langmuir and nucleation and growth kinetics are considered. However, it is clear that both processes are linked and affect each other. Several forms of mutual dependence were examined using the model as well as equations from ref 33 and some derivations from it. When these more elaborate models were used to fit the experimental data, the results obtained did not significantly improve the fit and the parameters obtained from it were essentially the same. For this reason, the simplified model, without mutual dependence of both processes, was chosen instead of more complex models.

Figure 5 shows the transient (full line) for a step from +0.898 to +0.938 V and the fit (dashed line) obtained to eq 1 with n = 3 (progressive nucleation). As can be observed, the model reproduces quite well the transient measurements. The only (small) deviations occur at short times, when double-layer charging processes affect the response. For all the curves with one shoulder, the best fit was obtained for n = 3, indicating that the nucleation and growth process proceeds through a progressive nucleation mechanism.

Processes following the BFT model should exhibit a linear dependence of $\log(t_{max})$ and $\log(j_{max})$ with potential according to the following relationship:[20,34]

$$\frac{\partial(\log j_{\max})}{\partial E} = -\frac{\partial(\log t_{\max})}{\partial E} \quad (2)$$

Figure 6 shows that both $\log(t_{max})$ and $\log(j_{max})$ are linear with potential for $E < +0.947$ V, which corresponds to $t_{max} > 0.13$ s and $j_{max} < 0.13$ mA/cm^2, respectively. The deviations from

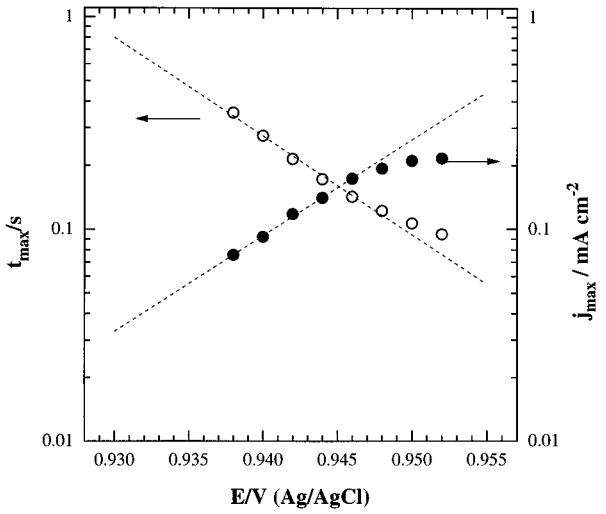

Figure 6. Plot of t_{max} (○) and j_{max} (●) vs electrode potential.

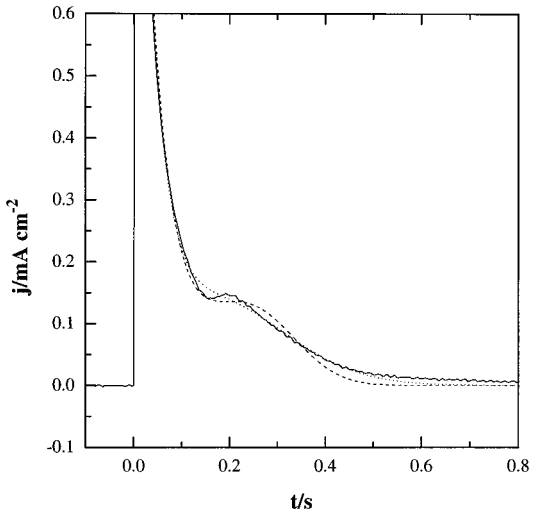

Figure 7. Current transient in 0.10 M H_2SO_4 + 1.0 mM Hg^{2+} for the adsorption process for a potential step from +0.968 to +0.912 V (full line) and fitted curves with progressive nucleation (dashed line) and instantaneous nucleation (dotted line).

linearity at shorter times are likely due to the influence of double-layer charging processes as mentioned above. The values of $\partial(\log t_{max})/\partial E$ and $\partial(\log j_{max})/\partial E$ obtained from Figure 6 are -49 ± 2 and 45 ± 2, respectively, fulfilling, within experimental error, eq 2 and thus providing additional evidence of the appropriateness of the model employed.

No attempt was made to fit the second shoulder that appears at potentials above +0.944 V since the small charge involved in this feature makes a reliable fit virtually impossible. However, this process is associated with the appearance of the sharp peak at the final stages of mercury desorption in the cyclic voltammogram. Once this latter process has taken place at +0.944 V, the mercury desorption process can be considered complete. As can be seen in the charge isotherm, no significant increase in the charge can be found beyond this point. The small change observed can be attributed to double-layer charging/discharging processes.

From Figure 5 it is also possible to determine the charge contribution of both processes to the total charge measured in the transient. The charge measured for the nucleation and growth process was 20 ± 2 μC cm^{-2}, regardless of the potential. This means that out of the total charge for the desorption process, 105 ± 5 μC cm^{-2}, only 20% of it corresponds to nucleation and growth processes. Taking this into account, we can then try to rationalize how the mercury desorption process takes place. As a starting point, we consider the ordered mercury bi-sulfate adlayer. The onset of the desorption process is +0.920 V. The initial stages of the mercury bi-sulfate adlayer desorption process occur via Langmuir kinetics. As a result, the desorption occurs randomly on the ordered adlayer. At this stage, the remaining part of the mercury bi-sulfate adlayer still retains its order. At +0.934 V, the mercury bi-sulfate adlayer is no longer stable, due to the numerous vacancies generated, and the order-to-disorder transition takes place. This transition implies the fast dissolution of the remaining mercury bi-sulfate adlayer, along with the adsorption of bi-sulfate anions which are present on the electrode surface at positive potentials. Once the mercury has been completely stripped from the electrode surface (at +0.944 V), the bi-sulfate adlayer undergoes a disorder−order transition that leads to the formation of the $(\sqrt{3}\times\sqrt{7})$ bi-sulfate structure.

As previously discussed an n value of 3 indicates that the process follows progressive nucleation, that is, the number of nuclei increases with time. Two different nucleation sites can be found on well-ordered single-crystal surfaces: terrace sites and defect sites. As the number of defects remains constant throughout an experiment, a nucleation process controlled by defect sites should follow an instantaneous nucleation ($n = 2$) mechanism. This was the case for Cu UPD on Au(111) electrodes in sulfuric acid solution as reported by Kolb et al.[20,21] However, in the present case, as the number of nuclei increases with time, the nucleation process cannot be due solely to defect sites but also to nucleation at random positions on the terraces. Considering that the initial desorption process follows a Langmuir isotherm, the areas of the electrode surface where nuclei are more likely to be formed are those that have a lower mercury bi-sulfate coverage.

A similar analysis can be carried out for the mercury deposition process. Figure 7 shows an adsorption transient recorded for a potential step from +0.968 to +0.912 V. This transient is very similar to those obtained for the desorption process, showing one clear shoulder. The second shoulder, the one corresponding to the initial process of the order-to-disorder transition in the bi-sulfate layer adsorbed on the electrode, is generally masked by the double-layer charging processes and the Langmuir isotherm, since the transition is fast and the charge associated with it is very small. In some cases (see for instance Figure 8), a small shoulder which we ascribe to this order-to-disorder transition can be seen at very short times.

Similar to the desorption transients, the capacitance curve obtained from the adsorption charge exhibits the same features as the voltammetric profile. Thus, the same analysis may be applied to these transients. However, neither the instantaneous nucleation (Figure 7, dotted line) nor the progressive nucleation (Figure 7, dashed line) models provided a good fit to the experimental curve. At this mercury concentration (1.0 mM Hg^{2+}) diffusion may still play a role in the process, affecting the kinetics of adsorption, as has been previously reported for lead UPD on Ag(111) electrodes for lead concentrations below 10^{-2} M.[19] Thus, transients were also recorded in 0.1 M H_2SO_4 + 0.01 M Hg^{2+} (Figure 8), where no transport limitations would be expected. In this case, we were able to fit the experimental data, and as for the desorption transients, the best fit was obtained with a progressive nucleation model ($n = 3$).

The increase in the mercury concentration causes an acceleration of the adsorption kinetics so that the potential region over which the analysis is applicable is limited. Therefore the

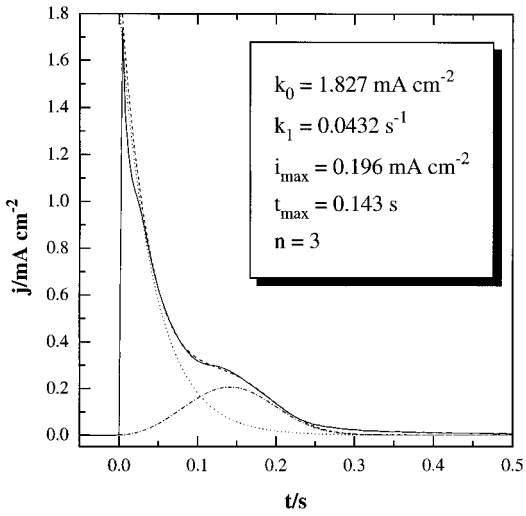

Figure 8. Current transient in 0.10 M H_2SO_4 + 10mM Hg^{2+} for mercury adsorption processes on a Au(111) electrode for a potential step from +0.968 to +0.912 V (full line) and fitted curve with a progressive nucleation model (dashed line). The dotted and dash-dotted lines represent the Langmuir and nucleation and growth terms, respectively. Values of the parameters obtained from the fitting are given in the inset.

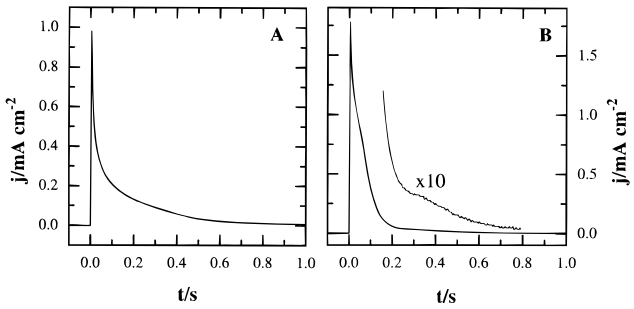

Figure 9. Current transients in 0.10 M $HClO_4$ + 1.0 mM NaCl + 1.0 mM Hg^{2+} for mercury desorption processes on a Au(111) electrode for potential steps from +0.898 to (A) +0.934 V and (B) +0.954 V. In the inset, the transient in (B) has been partially expanded (×10) to show the presence of a shoulder at ca. 0.35 s.

analysis based on values of t_{max} and j_{max} is no longer reliable. However, owing to the similarities between the adsorption and desorption processes, the application of the BFT model can be considered to be still valid.

For the mercury adsorption process, we propose that the formation of the mercury bi-sulfate is as follows. The initial stages of mercury deposition trigger an order−disorder transition in the $(\sqrt{3}\times\sqrt{7})$ bi-sulfate adlayer present on the electrode surface at +0.968 V. The mercury bi-sulfate pairs start adsorbing randomly on the electrode surface following Langmuir kinetics. At +0.920 V, the disorder−order transition in the mercury bi-sulfate layer takes place and the formation of the ordered adlayer reaches completion.

Current Transients in 0.1 M $HClO_4$ + 1.0 mM NaCl + 1.0 mM Hg^{2+}. Figure 9 shows two transients from an initial potential of +0.898 to +0.934 V (A) and +0.954 V (B), respectively, obtained in 0.1 M $HClO_4$ + 1.0 mM NaCl + 1.0 mM Hg^{2+}. Although the transients deviate from an ideal exponential decay, no clear shoulders were found. Only at potentials positive of +0.944 V was a small shoulder, similar to the one found in sulfuric acid, seen. (For example, the inset to Figure 9B shows a small shoulder when the current scale is expanded.) As was done in the previous case, the charge under all the transients was measured to give the charge isotherm

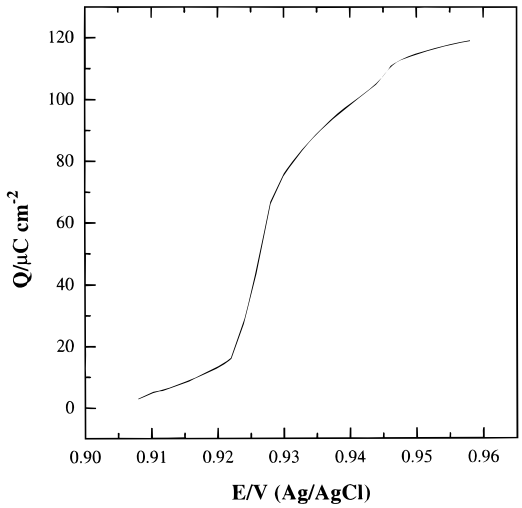

Figure 10. Charge isotherm obtained from the desorption current transients in 0.10 M $HClO_4$ + 1.0 mM NaCl +1.0 mM Hg^{2+}.

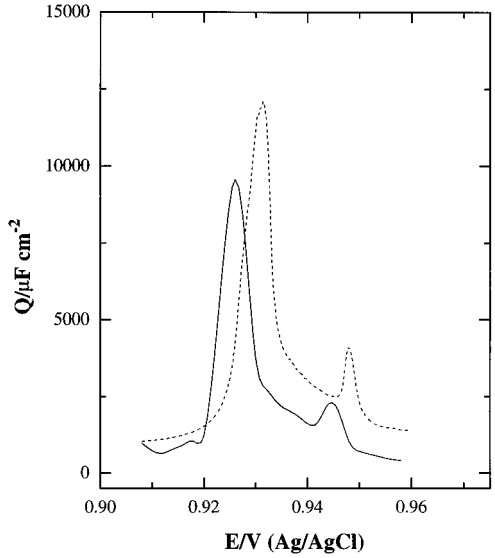

Figure 11. Capacitance profile from the charge isotherm (full line) and the voltammetric profile (dashed line) for mercury desorption in 0.10 M $HClO_4$ + 1.0 mM NaCl +1.0 mM Hg^{2+}.

(Figure 10). The capacitance curve obtained by differentiation agrees well with that obtained from the cyclic voltammogram (Figure 11). As before, there was a small shift toward negative potentials of the curve obtained from the transients, due to the quasi-equilibrium conditions present. The small shoulder appearing at potentials positive of +0.944 V again coincides with the peak potentials for the second peak in the capacitance curve, confirming that this shoulder is related to the formation of the ordered hexagonal overlayer structure in chloride media (at potentials where no mercury has been deposited).

Equation 1 did not provide a good fit to any of the desorption transients obtained in this medium. Moreover, the transients clearly deviate from the pure exponential decay of the Langmuir term. This indicates that the transients for the desorption of the mercury chloride adlayer follow neither Langmuir kinetics nor nucleation and growth processes. We believe that the absence of a nucleation and growth mechanism in the transient is a consequence of the absence of an ordered mercury chloride structure at potentials negative of the main UPD peaks.

On the other hand, the deviation from Langmuir kinetics indicates that other interactions, in addition to the gold surface−mercury interactions, play a role in the kinetics of the desorption

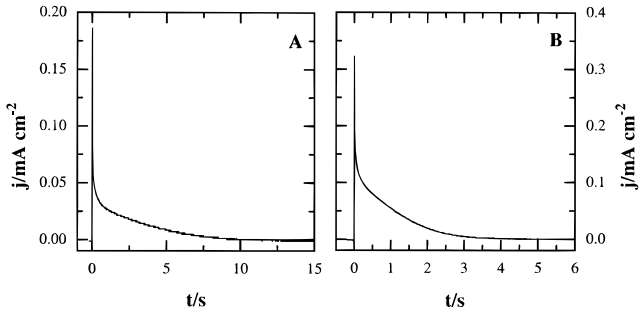

Figure 12. Current transients for mercury desorption processes on a Au(111) electrode for potential steps from +0.698 to (A) +0.778 V and (B) +0.808 V in 0.10 M CH_3COOH + 0.10 M CH_3COONa + 1.0 mM Hg^{2+}.

process. The voltammetric results show that in the presence of chloride the onset of mercury desorption is shifted toward positive potentials relative to pure perchloric acid solutions. This indicates that chloride anions enhance the stability of the adlayer, probably through attractive interactions in the adlayer. These attractive interactions would, in turn, result in the deviations from Langmuir kinetics observed in the transients.

A similar behavior was observed for the adsorption transients. As for desorption, the transients deviated from Langmuir behavior, but a nucleation and growth mechanism was not observed.

Current Transients in 0.1 M CH_3COOH + 0.1 M CH_3COONa + 1.0 mM Hg^{2+}. The cyclic voltammetric profile indicates that the process of mercury adsorption/desorption in this medium is kinetically slow, since the peak separation was about 50 mV even at a sweep rate of 1 mV s^{-1}. The slow kinetics are reflected in the current transients obtained in this medium. In the previous two cases, the current reached a steady state (1% of the peak current) in less than 1 s. Here, as can be seen in Figure 12, more than 10 s are required in some cases to reach such a steady state current. A very similar behavior was obtained for the adsorption transients.

Transients in this medium exhibited a clear deviation from Langmuir behavior, and there was no indication of the presence of a nucleation and growth mechanism for either the desorption or the adsorption process. Unlike the mercury adlayers in chloride medium, in acetate media we have found ordered adlayers (by X-ray diffraction) at potentials negative of the main UPD peak.[26] However, no sharp peaks, indicative of phase transitions, were observed in the cyclic voltammogram. Moreover, this ordered adlayer exhibits an irreversible compression with the applied potential, although no reflection of this behavior is evident in the cyclic voltammogram. These facts, together with the absence of a nucleation and growth mechanism in the kinetics, would indicate that no charge is involved in the phase transition that leads to the formation/disruption of the ordered adlayer.

The capacitance curve obtained from the transients shows a clear displacement of the desorption peak toward negative potentials relative to the cyclic voltammetric peak (Figure 13). As before, the capacitance curve from the transient is obtained under quasi-equilibrium conditions. The peak potential obtained (+0.755 V) corresponds to the mean potential value of the adsorption−desorption voltammetric peaks, as would be anticipated for a response obtained under quasi-equilibrium conditions.

4. Conclusions

Strongly interacting anions such as bi-sulfate, chloride, and acetate play important roles in the kinetics of mercury UPD on

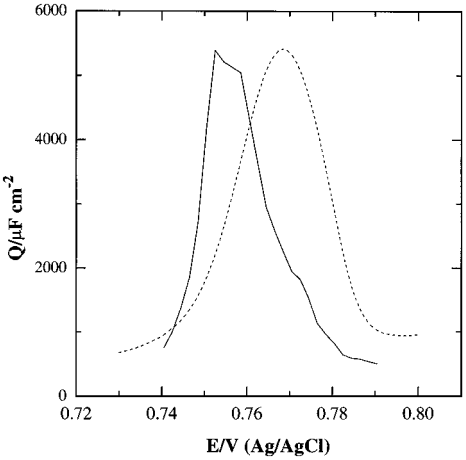

Figure 13. Capacitance profile from the charge isotherm (full line) and the voltammetric profile (dashed line) for mercury desorption in 0.10 M CH_3COOH +0.10 M CH_3COONa + 1.0 mM Hg^{2+}.

Au(111) electrodes. In the absence of strongly interacting anions, i.e., in perchloric acid, the mercury UPD process is largely controlled by mercury−gold surface interactions. The presence of sulfuric acid in the supporting electrolyte alters the kinetics of the initial and final stages of mercury deposition/dissolution. The presence of two well-ordered structures at potentials below (a mercurous sulfate $\sqrt{3}\times\sqrt{19}$ structure) and above (a $\sqrt{3}\times\sqrt{7}$ bi-sulfate structure) mercury deposition leads to the appearance of two pairs of sharp spikes in the cyclic voltammogram. Analysis of the current transients obtained for deposition and dissolution processes reveals that three different processes are taking place during the adsorption/desorption of the mercury bi-sulfate layer: adsorption/desorption processes governed by Langmuir kinetics, a nucleation and growth process linked to the order/disorder transition to form the mercury bi-sulfate adlayer and a order/disorder transition related to the formation/disruption of the $\sqrt{3}\times\sqrt{7}$ bi-sulfate layer.

In chloride medium, the voltammetric profile is very similar to that obtained in sulfuric acid solution, with the presence of two sharp spikes. However, previous X-ray measurements only revealed the presence of an ordered structure at potentials above the main UPD peak. Consequently, no nucleation and growth kinetics mechanism was found linked to the process of formation/disruption of the mercury chloride adlayer. The transients show a clear deviation from the ideal Langmuir behavior, probably linked to the presence of attractive interactions in the mercury chloride adlayer.

The kinetics of mercury UPD in acetate media are clearly slower than in the previous media, as revealed by voltammetric and chronoamperometric measurements. The slow kinetics appear to be related to the formation of Hg^{2+}−acetic acid complexes in solution. Although ordered structures are formed at potentials below the main UPD peaks, no nucleation and growth mechanism was observed. It is likely that the phase transition that leads to the formation/disruption of the ordered mercury acetate adlayer involves no significant charge transfer, and no signal from it is observed by electrochemical means.

These studies illustrate the delicate interplay between the presence of strongly interactive anions with kinetics and structure of phase transitions by electrochemical means.

Acknowledgment. This work was supported by the Office of Naval Research and the National Science Foundation. We thank Prof. J. M. Feliu for supplying the small gold electrodes used in this work and for valuable comments. E.H. acknowl-

edges support by a fellowship from the Ministry of Education and Science of Spain.

References and Notes

(1) Kolb, D. M. In *Advances in Electrochemistry and Electrochemical Engineering*; Gerischer, H., Tobias, C. W., Eds.; Wiley: New York, 1978; Vol. 11, p 125.

(2) Adzic, R. In *Advances in Electrochemistry and Electrochemical Engineering*; Gerischer, H., Tobias, C. W., Eds.; Wiley: New York, 1984; Vol. 13, p 159.

(3) Matsumoto, H.; Inukai, J.; Ito, M. *J. Electroanal. Chem.* **1994**, *379*, 223.

(4) Hachiya, T.; Honbo, H.; Itaya, K. *J. Electroanal. Chem.* **1991**, *315*, 275.

(5) Sashikata, K.; Furuya, N.; Itaya, K. *J. Electroanal. Chem.* **1991**, *316*, 361.

(6) Dietterle, M.; Will, T.; Kolb, D. M. *Surf. Sci.* **1995**, *342*, 29.

(7) Chen, C.-H.; Vesecky, S. M.; Gewirth, A. A. *J. Am. Chem. Soc.* **1992**, *114*, 451.

(8) Chen, C.-H.; Kepler, K. D.; Gewirth, A. A.; Ocko, B. M.; Wang, J. *J. Phys. Chem.* **1993**, *97*, 7290.

(9) Yee, H. S.; Abruña, H. D. *Langmuir* **1993**, *9*, 2460.

(10) Gómez, R.; Yee, H. S.; Bommarito, G. M.; Feliu, J. M.; Abruña, H. D. *Surf. Sci.* **1995**, *335*, 101.

(11) Yee, H. S.; Abruña, H. D. *J. Phys. Chem.* **1993**, *97*, 6278.

(12) Wang, J. X.; Adzic, R. R.; Ocko, B. M. *J. Phys. Chem.* **1994**, *98*, 7182.

(13) Toney, M. F.; Gordon, J. G.; Samant, M. G.; Borges, G. L.; Melroy, O. R.; Yee, D.; Sorensen, L. B. *J. Phys. Chem.* **1995**, *99*, 4733.

(14) Bewick, A.; Thomas, B. J. *Electroanal. Chem.* **1977**, *84*, 127.

(15) Schultze, J. W.; Dickerman, D. *Ber. Bunsen−Ges. Phys. Chem.* **1978**, *82*, 528.

(16) Schultze, J. W.; Dickerman, D. *Faraday Symp. Chem. Soc.* **1977**, *37*, 36.

(17) Staikov, G.; Jüttner, K.; Lorenz, W. J.; Schmidt, E. *Electrochim. Acta* **1978**, *23*, 305.

(18) Jovicevic, J. N.; Jovic, V. D.; Despic, A. R. *Electrochim. Acta* **1984**, *29*, 1625.

(19) Jovic, V. D.; Jovicevic, J. N.; Despic, A. R. *Electrochim. Acta* **1985**, *30*, 1455.

(20) Hölze, M. H.; Retter, U.; Kolb, D. M. *J. Electroanal. Chem.* **1994**, *371*, 101.

(21) Hölze, M. H.; Zwing, V.; Kolb, D. M. *Electrochim. Acta* **1995**, *40*, 1237.

(22) Chen, C.-H.; Gewirth, A. A. *Phys. Rev. Lett.* **1992**, *68*, 1571.

(23) Inukai, J.; Sugita, S.; Itaya, K. *J. Electroanal. Chem.* **1996**, *403*, 159.

(24) Li, J.; Abruña, H. D. *J. Phys. Chem. B* **1997**, *101*, 244.

(25) Li, J.; Abruña, H. D. *J. Phys. Chem. B.* **1997**, *101*, 2907.

(26) Li, J.; Herrero E.; Abruña, H. D. *J. Colloids Surf.*, accepted.

(27) Magnussen, O. M.; Ocko, B. M.; Adzic, R. R.; Wang, J. X. *Phys. Rev. B* **1995**, *51*, 5510.

(28) Herrero, E.; Abruña, H. D. *Langmuir* **1997**, *13*, 4446.

(29) Clavilier, J.; Armand, D.; Sun, S. G.; Petit, M. *J. Electroanal. Chem.* **1986**, *205*, 267.

(30) Martell, A. E.; Smith, R. M. *Critical stability constants*; Plenum Press: New York, 1977; Vol. 3.

(31) Bewick, A.; Fleischmann, M.; Thisks, H.R. *Trans. Faraday Soc.* **1962**, *58*, 2200.

(32) Fleischmann, M.; Thirsk, H. R. In *Advances in Electrochemistry and Electrochemical Engineering*; Delehay, P., Ed.; Wiley: New York; 1963; Vol. 3, p 123.

(33) Bosco, E.; Rangarajan, S. K. *J. Chem. Soc., Faraday Trans.* **1981**, *77*, 1673.

(34) Macdonald, D. D. *Transient Techniques in Electrochemistry*; Plenum: New York, 1977; p 277.